

Subject Section

A graph-based approach to diploid genome assembly

Shilpa Garg^{1,2,3,*}, Mikko Rautiainen^{1,2,3}, Adam M. Novak⁴, Erik Garrison^{5,6},
Richard Durbin^{5,6}, Tobias Marschall^{1,2,*}

¹ Center for Bioinformatics, Saarland University, Saarbrücken, Germany, ² Max Planck Institute for Informatics, Saarbrücken, Germany, ³ Saarbrücken Graduate School of Computer Science, Saarland University, Saarbrücken, Germany, ⁴ UC Santa Cruz Genomics Institute, University of California, Santa Cruz, US, ⁵ Wellcome Trust Sanger Institute, Hinxton, Cambridge, United Kingdom, ⁶ Department of Genetics, University of Cambridge, Cambridge, United Kingdom

*To whom correspondence should be addressed.

Associate Editor: XXXXXXX

Received on XXXXX; revised on XXXXX; accepted on XXXXX

Abstract

Motivation: Constructing high-quality haplotype-resolved *de novo* assemblies of diploid genomes is important for revealing the full extent of structural variation and its role in health and disease. Current assembly approaches often collapse the two sequences into one haploid consensus sequence and, therefore, fail to capture the diploid nature of the organism under study. Thus, building an assembler capable of producing accurate and complete diploid assemblies, while being resource-efficient with respect to sequencing costs, is a key challenge to be addressed by the bioinformatics community.

Results: We present a novel graph-based approach to diploid assembly, which combines accurate Illumina data and long-read Pacific Biosciences (PacBio) data. We demonstrate the effectiveness of our method on a pseudo-diploid yeast genome and show that we require as little as 50× coverage Illumina data and 10× PacBio data to generate accurate and complete assemblies. Additionally, we show that our approach has the ability to detect and phase structural variants.

Availability: <https://github.com/whatshap/whatshap>

Contact: {sgarg|t.marschall}@mpi-inf.mpg.de

1 Introduction

There are two homologous copies of every chromosome, one from each parent, in human and other diploid eukaryotic genomes. Determining the two genome sequences of those organisms per chromosome is important in order to correctly understand allele-specific expression and compound heterozygosity, and in order to carry out many analyses in the genetics of common diseases and in population genetics (Tewhey *et al.*, 2011; Glusman *et al.*, 2014). Furthermore, separate determination of the two haplotype sequences can in principle avoid genotyping errors in complex regions of the genome caused by simplistic models that treat variants at nearby sites as being independent.

The process of assembling two distinct genome sequences from sequencing reads in a haplotype-aware manner is known as *diploid* or *haplotype-aware genome assembly* and the assembled sequences are known as “haplotigs”. However, next generation sequencing (NGS)

reads are generally of short length and contain errors; therefore, solving the diploid genome assembly problem is fundamentally challenging. Additional challenges inherent in the genome assembly problem include dealing with short and long genomic repeats, handling general rearrangements present in the genome, and scaling efficiently with input size, genome size, and hardware availability.

Over the last decade, the development of various NGS technologies has impacted the assembly problem. In theory, the problem of *de novo assembly*—computing the consensus of two or more sequences—is NP-hard, when the problem is modelled either with string graphs or with de Bruijn graphs (Medvedev *et al.*, 2007). In the past decades, a multitude of heuristic approaches to haploid *de novo* assembly have been proposed (Idury and Waterman, 1995; Myers, 1995, 2005; Pevzner *et al.*, 2001; Nagarajan and Pop, 2009, 2013; Sović *et al.*, 2013).

However, even with Sanger (reads of the order of 800-1000 base pairs) and Illumina sequencing, which deliver short reads with low error rates, assembly of heterozygous diploid genomes has been a difficult

problem (Vinson *et al.*, 2005; Levy *et al.*, 2007). In practice, there are several short-read assemblers based on Illumina data for heterozygous genomes (Kajitani *et al.*, 2014; Pryszcz and Gabaldón, 2016; Simpson and Durbin, 2012; Bankevich *et al.*, 2012; Li, 2015b). The assemblies that they produce are accurate, but contain gaps and are composed of relatively short contigs and scaffolds. Third generation sequencing technologies such as methods available from Pacific Biosciences (PacBio) and Oxford Nanopore Technologies (ONT) deliver much longer reads, but with high error rates. There are now several long-read assemblers (Koren *et al.*, 2017; Vaser *et al.*, 2017; Xiao *et al.*, 2016; Berlin *et al.*, 2015; Chin *et al.*, 2013; Hunt *et al.*, 2015; Lin *et al.*, 2016) that use these long-read data for *de novo* assembly. The assemblies that are delivered from these assemblers are more contiguous, with longer contigs and scaffolds. Finally, there are hybrid assemblers that take advantage of long-read data (with its high error rate) and short-read data (with its low error rate) (Bashir *et al.*, 2012; Antipov *et al.*, 2015; Zimin *et al.*, 2017) and attempt to combine the best aspects of both. These hybrid assemblers have the potential to deliver highly accurate, repeat-resolved assemblies.

However, across the short, long, and hybrid categories, most assemblers require collapsing the two genome sequences of a diploid sample into a single haploid “consensus” sequence (or primary contig). The consensus sequence is obtained by merging the distinct alleles at regions of heterozygosity into a single allele, and therefore losing a lot of information. The resulting haploid *de novo* assembly does not represent the true characteristics of the diploid input genome.

Current approaches to reconstruct diploid genomes usually rely on collapsing assembly graphs to haploid contigs in intermediate steps (contig-based assembly) (Chin *et al.*, 2016; Pendleton *et al.*, 2015; Seo *et al.*, 2016; Mostovoy *et al.*, 2016), or on using a reference genome to partition the reads by haplotype (reference-guided assembly) (Glusman *et al.*, 2014; Martin *et al.*, 2016; Chaisson *et al.*, 2017b). In both types of approaches, the reads are first aligned (either to the reference genome or the contigs). Second, variants such as SNVs are called based on the aligned reads. Finally, the detected variants are phased using long reads from either the same or a different sequencing technology. Because these methods represent the genome with haploid sequences in some processing steps, we refer to them as *linear* approaches.

For both reference-guided and contig-based assembly, this third step—solving the phasing problem—has been formulated as the minimum error correction (MEC) optimization problem (Lippert *et al.*, 2002; Cilibrasi *et al.*, 2007). The reviews by Rhee *et al.* (2016) and Klau and Marschall (2017) provide introductions to this formulation. There are several disadvantages to reference-guided assembly; for example, the reads are initially aligned to the reference genome and therefore the process contains reference bias. Also, this approach can fail to detect sequences or large structural variants that are unique to the genome being assembled.

However, there are also several reasons why the set of sequences/contigs produced by contig-based assembly is not ideal. First, the contigs produced by haploid assemblers ignore the heterozygous variants in complex regions, opting instead to break contiguity to express even moderate complexity. Second, the contigs do not capture end-to-end information in the genome; the ordering or relationships between contigs are critical in order to generate end-to-end chromosomal-length assemblies.

One example of a newer diploid assembly method is Weisenfeld *et al.* (2017), where 10x Genomics linked read data is used to determine the actual diploid genome sequence. Their approach is based on de Bruijn graphs and applies a series of graph simplifications, where simple bubbles are detected and phased by using (short) reads that stem from the same (long) input molecule, which is determined through barcoding. There is also a recent study by Chin *et al.* (2016), who follow a linear phasing

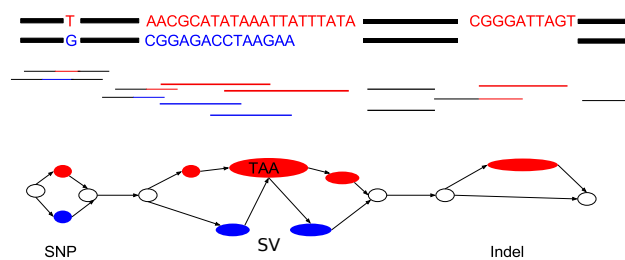


Fig. 1. Based on reads (middle) from the two sequences (top), the bubbles in the graph (bottom) show three different heterozygous variants; the first one is an SNV, the second one is an SV, and the third one is an indel.

approach to generate diploid assemblies (*haplotigs*) for diploid genomes by using PacBio reads.

Contributions. We propose a graph-based approach for generating haplotype-aware assemblies of single individuals. Our contribution is twofold. First, we propose a hybrid approach, integrating accurate Illumina and long PacBio reads in order to generate diploid assemblies. The Illumina reads are used to generate an assembly graph that serves as a backbone for subsequent PacBio-based steps. Second, we generalize the diploid assembly problem to encompass constructing the diploid assembly directly from the underlying assembly graph and thereby avoid “flattening” the assemblies to linear sequences at any time. The two haplotype sequences can be seen as two paths over the regions of heterozygosity in the assembly graph.

Phasing using an assembly graph has several advantages over linear approaches. In particular, it allows us to represent and phase heterozygous structural variants (SVs), which are represented by bubbles in the assembly graph. A bubble is defined as a set of disjoint paths that share the same start and end nodes. Figure 1 illustrates how such bubbles can represent both small variants (which we define as SNVs and indels up to 50 base pairs in length) and larger structural variants. Handling small variants and SVs in a unified way facilitates phasing larger blocks because haplotype reconstruction is not disrupted by SVs. Figure 2 illustrates this conceptual advantage. The figure shows four SNVs separated by two large SVs, and six reads spanning these variants. Out of those reads, the two reads r_3 and r_4 span the two SVs, but do not cover any of the two SNVs. Conversely, the reads which cover the SNVs on either side do not cover the SVs. In this case, Falcon Unzip generates a primary contig that spans from one end to the other, but generates incomplete and fragmented haplotigs (phased primary contigs in the language of Falcon Unzip) covering only the SNVs. By contrast, our graph-based approach attempts to phase across all types of variation, including SVs.

We demonstrate the feasibility of our approach by performing a haplotype-aware *de novo* assembly of a whole pseudo-diploid yeast (SK1+Y12) genome. We show that we generate more accurate and more contiguous phased diploid genomes compared to Falcon Unzip. Through empirical testing with different input coverage levels, we demonstrate that we require only $50\times$ short-read coverage and as little as $10\times$ long-read coverage data to generate diploid assemblies. This illustrates that our hybrid strategy is a cost-effective way of generating haplotype-resolved assemblies. Finally, we show that we successfully detect and phase large structural variants.

2 Diploid assembly pipeline

Our assembly workflow uses short read (e.g. Illumina) and long read (e.g. PacBio) data in combination, as illustrated in Figure 3. We describe the details of this process below.

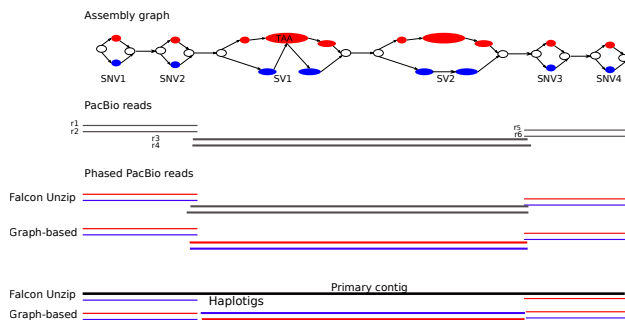


Fig. 2. Input: an assembly graph (top) (consisting of four SNVs and two SVs) and the PacBio reads $r_1, r_2, r_3, r_4, r_5, r_6$ (gray). Output: the phased reads (colored in blue and red) and haplotigs (bottom) using Falcon Unzip and our approach. Our graph-based approach also phases the central region. Contrarily, Falcon Unzip does not phase it, and so the region does not contribute to the total haplotig size.

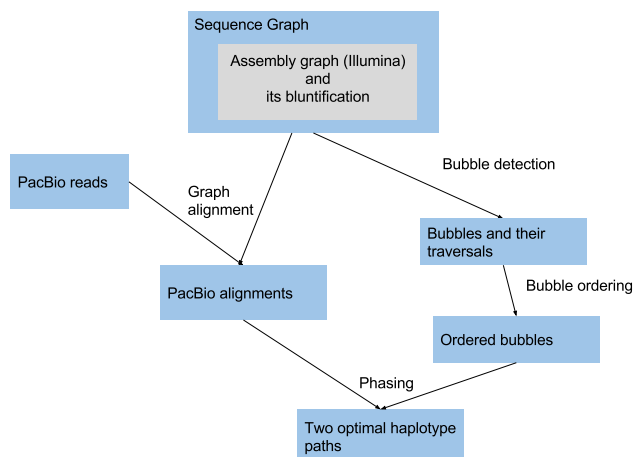


Fig. 3. Overview of the diploid assembly pipeline.

2.1 Sequence graph

Our first step is to construct a sequence graph using short read data with a low error rate, as provided by the Illumina platform.

Definition 1 (Sequence Graph). We define a sequence graph $G_s(N_s, E_s)$ as a bidirected graph, consisting of a set of nodes N_s and a set of edges E_s . The nodes n_i are sequences over an alphabet $\mathcal{A} = \{A, C, G, T\}$. For each node $n_i \in N_s$, its reverse-complement is denoted by n'_i . An edge $e_{i,j}$ connects the nodes n'_i to n_j . Nodes may be traversed in either the forward or reverse direction, with the sequence being reverse-complemented in the reverse direction.

In words, edges represent adjacencies between the sequences of the nodes they connect. Thus, the graph implicitly encodes longer sequences as the concatenated sequences of the nodes along walks through the graph.

To illustrate this, we consider an example sequence graph G_s in Figure 4. It consists of a node set $N_s = \{1, 1', 2, 2', 3, 3', \dots\}$ and an edge set $E_s = \{1 \rightarrow 2', 1 \rightarrow 3' \dots\}$.

To generate the sequence graph G_s , we first employ SPAdes (Bankevich *et al.*, 2012), which constructs and simplifies a de Bruijn graph, and we subsequently remove the overlaps between the nodes in the resulting graph in a process we call *bluntification*, explained in the Supplement.

2.2 Bubble detection in sequence graphs

To account for heterozygosity in a diploid genome, we perform bubble detection. The notion of *bubble* we use is closely based on the *ultrabubble* concept as defined by Paten *et al.* (2017). Briefly, bubbles have the following properties:

- **2-node-connectivity.** A bubble is bounded by fixed start and end nodes. Removing both the start and end nodes disconnects the bubble from the rest of the graph. Note that a bubble can be viewed in either orientation. If the graph is traversed in one direction, and a bubble is encountered that starts at a node n_i and ends at a node n'_j , then that bubble can also be described as the bubble with start node n_j and end node n'_i , as it would be encountered when traversing the graph in the opposite direction.
- **Directed acyclicity.** A bubble is directed and acyclic.
- **Directionality.** All paths through the bubble flow from start to end.
- **Minimality.** No vertex in the bubble other than the start node n_i (with proper orientation) forms a pair with the end node n'_j (with proper orientation) that satisfies the above properties. Similarly, no vertex in the bubble other than n'_j forms such a pair with n_i .

A bubble can represent a potential sequencing error or genetic variation within a set of homologous molecules. We represent bubbles as collections of alternative paths.

Definition 2 (Path). We define path a_i as a linear ordering of nodes $a_i = n_1, \dots, n_m$.

A bubble is a collection of paths with the same start and end node and can be defined as follows:

Definition 3 (Bubble). Formally, a bubble is represented as a collection of allele paths $l_k = \{a_1, a_2, \dots\}$ where

$$a_1 = (n_1, n_2, \dots, n_m), a_2 = (n_1, n_3, \dots, n_m)$$

and so on.

For example, Figure 4 shows a set of two bubbles $L = \{l_2, l_1\}$, and the set of allele paths for the bubble l_2 is $\{a_1, a_2, a_3\}$, where $a_1 = (6, 7', 8', 11')$, $a_2 = (6, 9', 11')$, $a_3 = (6, 10, 11')$.

2.3 PacBio alignments

For phasing bubbles, we consider long reads from third generation sequence technologies such as PacBio. We align these long reads to the sequence graph G_s to generate paths through the graph. We perform graph alignment using a banded version of the algorithm described by Rautiainen and Marschall (2017), which is a generalization of semi-global alignment to sequence-to-graph alignment¹.

There are several advantages of aligning PacBio reads to graphs instead of to a reference genome or contigs. SNPs often occur near larger variants such as insertions and deletions. SNPs are thus often missed in these regions when reads contain large mismatches with respect to the linear sequences they are aligned against. Graph alignment allows the alignment of reads to variants appropriate to each read's phase, and to other types of complex events.

Definition 4 (Alignment). We define a set of read alignments as $R = \{r_1, r_2, \dots, r_j\}$, where each read alignment r_j is given by a path of oriented nodes in graph G_s , written $r_j = (n_1, \dots, n_m)$.

For example, in Figure 4, $R = \{r_1, r_2, r_3, r_4\}$ and the read alignment path r_1 can be written as $r_1 = (1, 2', 5', 6, 7', 8', 11')$

¹ <https://github.com/maickrau/GraphAligner>

2.4 Bubble ordering

The next stage of our algorithm is to obtain an ordering of the bubbles $L = (l_1, l_2, \dots, l_k)$, which we refer to as a *bubble chain*. For example, in Figure 4, $L = (l_1, l_2)$ is a bubble chain. A general sequence graph G_s is cyclic, due to different types of repeats present in the genome that create both short and long cycles. Ordering bubbles in such a graph is closely related to resolving repeats, which is a challenging problem. In this study, we rely on the Canu algorithm (Koren *et al.*, 2017) to provide a bubble ordering by aligning Canu-generated contigs to our sequence graph. Furthermore, we detect repetitive bubbles—that is, bubbles that would need to be traversed more than once in a final assembly—based on the depth of coverage of aligned PacBio reads, and remove such bubbles. We deem a bubble repetitive if the number of PacBio reads aligned to its starting node is greater than a coverage threshold specified by the user over the genome. For example, given a $30\times$ ($=c$) data set and a repeat that occurs 20 ($=r$) times in the genome, then the coverage at the bubble on average is 600 ($=r \cdot c$).

2.5 Graph-based phasing

Given a sequence graph G_s , ordered bubbles L , and PacBio alignments R , the goal is to reconstruct two haplotype sequences $\{h_0, h_1\}$, called haplotigs, along each chain of bubbles.

Definition 5 (Haplotype path). *Formally, a pair of haplotype paths (h_0, h_1) can be defined as two paths through a bubble chain in the sequence graph and denoted as:*

$$\begin{aligned} h_0 &= (n_s, n_2, \dots, n_e) \\ h_1 &= (n_s, n_3, \dots, n_e) \end{aligned}$$

where h_0 and h_1 may differ at the heterozygous regions defined by bubbles, and n_s and n_e are the start and end of the bubble chain.

The two genome sequences can be seen as two walks through the bubbles L in the sequence graph G_s that are consistent with the PacBio alignments R . In maximum likelihood terminology, the goal is to find the most likely haplotype paths given the alignment paths traversing through the bubbles. For example, in Figure 4, given bubbles (l_1, l_2) and PacBio alignments $R = \{r_1, r_2, r_3, r_4\}$, the goal is to find two maximum likelihood haplotype paths $\{h_0, h_1\}$ such that each PacBio alignment is assigned to one of the haplotypes.

For a linear chain of bubbles L , the task of finding these two haplotype paths is equivalent to picking one allele path per haplotype for each bubble. To this end, we note that an alignment path r_j for a given read can be viewed as a sequence of allele paths traversed in consecutive bubbles. We represent this association of reads to allele paths in the form of a *bubble matrix* $\mathcal{F} \in \{0, 1, \dots, m, -\}^{|R| \times |L|}$, where $|R|$ is the number of reads, $|L|$ is the number of bubbles along a chromosome, and $m = \max_k |l_k|$ is the maximum number of paths (or alleles) in any bubble $l_k \in L$. The entry $\mathcal{F}(j, k) \in \{0, 1, \dots, m, -\}$ represents the allele path index in bubble l_k that read r_j is aligned to, where a value of “-” indicates that the read does not cover the bubble. In Figure 4, note that the read alignment path r_4 does not cover all the nodes in any of the allele paths in l_2 and hence we set the corresponding value $\mathcal{F}(4, 2)$ to “-”. As a result, this read covers only one bubble, which renders it uninformative for phasing, and we do not consider it further. The remaining phasing-informative reads in Figure 4 are represented as:

$$\mathcal{F} = \begin{matrix} & l_1 & l_2 \\ \begin{matrix} r_1 \\ r_2 \\ r_3 \end{matrix} & \begin{pmatrix} 0 & 0 \\ 2 & 2 \\ 1 & 2 \end{pmatrix} \end{matrix} \quad (1)$$

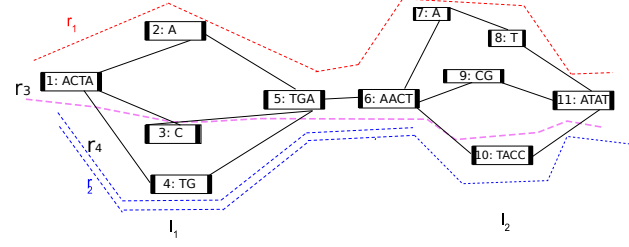


Fig. 4. For a subgraph of G_s , the example shows two bubbles l_1 and l_2 , and their corresponding alleles. Reads r_1, r_2, r_3, r_4 traverse the bubbles.

Corresponding to \mathcal{F} , we have a weight matrix $\mathcal{W} \in W^{|R| \times |L| \times m}$. Each entry in $\mathcal{W}(j, k)$ is a tuple storing a weight for each allele, which can for instance reflect “phred-scaled” (i.e. $-10 \log(p)$) probabilities that the read supports a given allele. The weight of “0” at the i^{th} entry in the tuple $\mathcal{W}(j, k)$ encodes that the read r_j is aligned to allele path index i in bubble l_k . The remaining non-zero values in tuple $\mathcal{W}(j, k)$ store the confidence scores of switching the aligned read r_j to other alleles in bubble l_k .

For example, the corresponding weight matrix $\mathcal{W}(j, k)$ for \mathcal{F} (1) is given by:

$$\mathcal{W} = \begin{matrix} & l_1 & l_2 \\ \begin{matrix} r_1 \\ r_2 \\ r_3 \end{matrix} & \begin{pmatrix} [0, q_1, q_2] & [0, q_3, q_4] \\ [q_9, q_8, 0] & [q_{11}, q_5, 0] \\ [q_{10}, 0, q_7] & [q_5, q_6, 0] \end{pmatrix} \end{matrix} \quad (2)$$

where the entry $\mathcal{W}(1, 1)$ value $[0, q_1, q_2]$ means that the read r_1 is aligned to allele a_0 at bubble l_1 . Additionally, the cost of flipping it to other alleles is q_1 for a_1 and q_2 for a_2 .

We are now ready to present the problem formulation. The main insight is that solving phasing for bubble chains is similar to solving the phasing problem for multi-allelic SNVs in reference-based haplotype reconstruction. Therefore, we build on the previous formulation of the Minimum Error Correction (MEC) problem (Lancia *et al.*, 2001) and its weighted version (wMEC) (Lippert *et al.*, 2002; Patterson *et al.*, 2014) and further adapt it to work on a subgraph consisting of a chain of bubbles, defining the *Minimum Error Correction for graphs* (gMEC) problem.

Problem 1 (wMEC for bubble chains (gMEC)). *Assume we are given a bubble chain $L = (l_1, \dots, l_{|L|})$ and a set R of aligned reads r_j that pass through these bubbles, with $\mathcal{F}(j, k)$ indicating the index of the allele in bubble l_k that the alignment of read r_j passes through, or “-” if it does not pass through l_k , and that $\mathcal{W}(j, k, i)$ is the cost of flipping $\mathcal{F}(j, k)$ to new value i . We want to find two paths through L , each of which consists of a sequence of allele indices specifying which allele the path takes in each bubble l_k , and then to flip entries of \mathcal{F} such that each row is equal to one of the paths for all non-dash entries while the incurred costs are minimized.*

Note that the wMEC problem constitutes a special case of gMEC, where the input graph is a chain of bi-allelic bubbles. Next, we describe how to solve gMEC via dynamic programming (DP).

In the WhatsHap algorithm (Patterson *et al.*, 2014), wMEC is solved in an exact manner for bi-allelic variants using a dynamic programming approach. It runs in $\mathcal{O}(2^c \cdot |L|)$ time, where $|L|$ is the number of variants to be phased and c is the maximum physical coverage. The basic idea is to proceed column-wise from left to right over a set of active reads. Each read remains active from its first non-dash position to its last non-dash position in \mathcal{F} . In column k , we denote the set of active reads as $A(k)$, particularly, $c = \max_k \{|A(k)|\}$. The algorithm now considers all *bipartitions* of $A(k)$, that is, all pairs $B = (P, Q)$ of disjoint sets P and Q such that

$P \cup Q = A(k)$. We fill a DP table column wise and for each column k of \mathcal{F} , we fill a DP table column $C(k, \cdot)$ with $2^{|A(k)|}$ entries corresponding to these bipartitions of $A(k)$. Each entry $C(k, B)$ is equal to the cost of solving wMEC on the partial matrix consisting of columns 1 to k of \mathcal{F} such that the bipartition of the full read set $A(1) \cup \dots \cup A(k)$ extends B according to the below definition.

Definition 6 (Bipartition extension). For a given set A and a subset $A' \subset A$, a bipartition $B = (P, Q)$ of A is said to extend a bipartition $B' = (P', Q')$ of A' if $P' \subset P$ and $Q' \subset Q$.

Once all entries of the DP table have been computed, the minimum of the last column $\min_B \{C(|L|, B)\}$ indicates the optimal wMEC cost and the optimal bipartition can be obtained by backtracing. We refer the reader to Patterson *et al.* (2014) for a more detailed explanation of this algorithm.

Solving gMEC for bubble chains. The basic idea is to now extend the dynamic program to consider all possible path-pairs through each bubble. In the bi-allelic case, we have only two paths in every bubble and, therefore, there is only one pair of distinct paths. In the multi-allelic case, we consider all possible path pairs in each bubble. The goal is to find an optimal pair of paths from the sequence graph G_s . Analogously to the WhatsHap algorithm for wMEC, we proceed from left to right using dynamic programming.

To explain the dynamic programming algorithm that we use, consider a toy example with the weight matrix (2):

$$\mathcal{W} = \begin{matrix} & l_1 & l_2 \\ \begin{matrix} r_1 \\ r_2 \\ r_3 \end{matrix} & \begin{pmatrix} [0, 10, 5] & [0, 5, 8] \\ [7, 6, 0] & [5, 2, 0] \\ [2, 0, 4] & [4, 3, 0] \end{pmatrix} \end{matrix} \quad (3)$$

DP cell initialization. Along similar lines as Patterson *et al.* (2014), we first compute the local cost incurred by bipartition $B = (R, S)$ in column k , denoted $\Delta_C(k, B)$, and later combine it with the corresponding costs incurred in previous columns. The cost $W_{k,R}^i$ of flipping all entries in a read set R to an allele index $i \in \{0, 1, \dots, |l_k|\}$ is given by

$$W_{k,R}^i = \sum_{j \in R} [\mathcal{F}(j, k) \neq i] \cdot \mathcal{W}(j, k, i),$$

In the same manner, we can compute costs $W_{k,S}^i$ for read set S to an allele index i .

To compute the cost incurred by a bipartition in a particular column k , we minimize over all possible pairs of alleles in bubble l_k . There are $\binom{|l_k|}{2}$ such pairs. So given the corresponding column vectors $\mathcal{F}(k)$ and $\mathcal{W}(k)$ of the bubble matrix and of the weight matrix, respectively, and the bipartition $B = (R, S)$ of active reads $A(k)$, the cost $\Delta_C(k, B)$ is computed by minimizing over all pairs of alleles $A = \{(x, y) \in l_k \times l_k | x \neq y, x < y\}$:

$$\Delta_C(k, B) = \min_{(p_0, p_1) \in A} \left\{ \min \{W_{k,S}^{p_0} + W_{k,R}^{p_1}, W_{k,S}^{p_1} + W_{k,R}^{p_0}\} \right\}, \quad (4)$$

where the outer minimization considers all allele pairs and the inner minimization considers the two possibilities of assigning those two alleles to the two haplotypes.

DP column initialization. We initialize the first DP column by setting $C(1, B) := \Delta_C(1, B)$ for all possible bipartitions B . We enumerate all bipartitions in Gray code order, as done previously in Patterson *et al.* (2014). This ensures that only one read is moved from one set to another in each step, facilitating constant time updates of the values $W_{k,S}^i$.

For a variant matrix (1) and its corresponding weight matrix (3), the DP column cell for bipartition $B = (R, S)$ is given by

$$\Delta_C(k, (R, S)) = \min \{W_{k,R}^0 + W_{k,S}^1, W_{k,R}^1 + W_{k,S}^2, W_{k,R}^0 + W_{k,S}^2, W_{k,R}^1 + W_{k,S}^0, W_{k,R}^2 + W_{k,S}^1, W_{k,R}^2 + W_{k,S}^0\}$$

Now, plugging values from (3) into the above equation for different bipartitions, $\Delta_C(1, \cdot)$ can be filled as follows:

$$\Delta_C(1, (\{r_1, r_2, r_3\}, \emptyset)) = \min\{9+0, 16+0, 9+0, 16+0, 9+0, 9+0\} = 9$$

Similarly, we can compute $\Delta_C(1, \cdot)$ for other bipartitions $(\{r_1, r_2\}, \{r_3\})$, $(\{r_1, r_3\}, \{r_2\})$, $(\emptyset, \{r_1, r_2, r_3\})$, $(\{r_3\}, \{r_1, r_2\})$, $(\{r_2\}, \{r_1, r_3\})$.

Input : Set $A(1)$ of reads covering bubble l_1 .

Output: $C(1, \cdot)$

for all bipartitions B of column k **do**

 Compute $\Delta_C(k, B)$ using Equation 4 and store in $C(1, B)$.

end

Algorithm 1: DP COLUMN INITIALIZATION

Due to the use of the Gray code order, we can perform this operation for one DP column in $\mathcal{O}(\binom{|l_k|}{2} \cdot 2^{|A(k)|})$ time.

DP column recurrence. Note that $C(k, B)$ is the cost of an optimal solution of Problem 1 for input matrices restricted to the first k columns under the additional constraint that the solution's bipartition of the full read set extends B . Since column k lists all bipartitions, the optimal solution to the input matrix consisting of the first k columns would be given by the minimum in that column. To compute entries in column $C(k+1, \cdot)$, we add up local costs incurred in column $k+1$ and costs from the previous column (see Algorithm 2). To adhere to the semantics of $C(k+1, B)$ described above, only entries in column k whose bipartitions are compatible with B are to be considered as possible "predecessors" of $C(k+1, B)$.

Definition 7 (Bipartition compatibility). For bipartitions $B = (P, Q)$ of A and $B' = (P', Q')$ of A' , B and B' are compatible if $P \cap A \cap A' = P' \cap A \cap A'$ and $Q \cap A \cap A' = Q' \cap A \cap A'$, denoted by $B \simeq B'$.

For example, consider the second column from (1) and (3). Let us compute $C(2, \cdot)$ for different bipartitions using recurrence in Algorithm 2:

$$C(2, (\{r_1, r_2, r_3\}, \emptyset)) = \min\{9+0, 10+0, 9+0, 10+0, 8+0, 8+0\} + \min\{C(1, (\{r_1, r_2, r_3\}, \emptyset)) = 8+9 = 17$$

To fill DP column $C(2, \cdot)$, we can analogously compute this for the remaining bipartitions $(\{r_1, r_2\}, \{r_3\})$, $(\{r_1, r_3\}, \{r_2\})$, $(\emptyset, \{r_1, r_2, r_3\})$, $(\{r_3\}, \{r_1, r_2\})$, and $(\{r_2\}, \{r_1, r_3\})$.

Backtracing. We can backtrace from the last column $C(|L|, \cdot)$ to compute an optimal bipartition $B = (R, S)$ of all input reads. Given this bipartition, we obtain minimum-cost haplotypes as follows: Let $B_k = (R_k, S_k)$ with $R_k = R \cap A(k)$ and $S_k = S \cap A(k)$ be the induced bipartition in column k . We then set

$$h_0(k) = a_i \quad \text{with } i := \operatorname{argmin}_{i' \in \{0, 1, \dots, |l_k|\}} W_{k,R_k}^{i'},$$

$$h_1(k) = a_j \quad \text{with } j := \operatorname{argmin}_{j' \in \{0, 1, \dots, |l_k|\}} W_{k,S_k}^{j'},$$

where a_i and a_j refer to the corresponding allele paths of bubble k (see Definition 2).

Input : $C(1, \cdot)$ for all bipartitions of bubble k .
Output: $C(k, \cdot)$ for all the columns k up to the last column $|L|$
for all columns $k \in \{2 \dots |L|\}$ **do**
 for all bipartitions $B \in \mathcal{B}(A(k))$ **do**
 Compute $\Delta_C(k, B)$ using Equation 4.
 Combine it with cost from column $k - 1$ to obtain cost for column k :

$$C(k, B) = \Delta_C(k, B) + \min_{B' \in \mathcal{B}(A(k-1)): B \simeq B'} C(k-1, B')$$

 end
 where $\mathcal{B}(A(k))$ denotes the set of all bipartitions of $A(k)$.
end

Algorithm 2: DP TABLE

Time complexity. Computing one DP column takes $\mathcal{O}(\binom{m}{2} \cdot 2^{|A(k)|})$ time, and the total running time is $\mathcal{O}(\binom{m}{2} \cdot 2^{|A(k)|} \cdot |L|)$ for $|L|$ bubbles, where m is the maximum number of alleles in any bubble from L . Running time is independent of read-length and, therefore, the algorithm is suitable for the increased read lengths available from upcoming sequencing technologies.

2.6 Generation of final assemblies

To generate final assemblies, for every connected component in the base sequence graph G_s , we traverse along the haplotype paths (h_0, h_1) running through that component. For the nodes in each path, we concatenate together the nodes' sequences from the base sequence graph G_s (in either in their forward or reverse-complement orientations, as specified by the path) in order to generate the final haplotig sequences.

3 Datasets and experimental setup

To evaluate the performance of our method, we consider the real data available from two haploid yeast strains SK1 and Y12 (Yue *et al.*, 2017), which we combine to generate a pseudo-diploid yeast. Both the SK1 and Y12 yeast strains are deeply sequenced using Illumina and PacBio sequencing. The Illumina dataset is sequenced to an average coverage of $469\times$ with 151 bp paired end reads. We randomly downsample the dataset to a lower average coverage of $50\times$. The PacBio data is sequenced to an average coverage of $334\times$ with an average read length of 4510 bp. For coverage analysis, we randomly downsample the PacBio reads to obtain datasets of different coverages $10\times$, $20\times$ and $30\times$ with their average read-lengths of 4482, 4501 and 4516 bp respectively.

3.1 Pipeline implementation

Sequence graph. The first step in our pipeline is to perform error correction on the Illumina data by using BFC (Li, 2015a), which, in our experience, retains heterozygosities well for diploid genomes. BFC is used with default parameters and provided with a genome size of 12.16 Mbp. The second step is to generate a sequence graph that includes heterozygosity information. To construct such a graph, we first construct the assembly graph by using a modified version of SPAdes v3.10.1 (Bankevich *et al.*, 2012). We modify the original SPAdes to skip the bubble removal step and retain the heterozygosity information in the graph, and run it with default parameters plus the `--only-assembler` option. It uses the short Illumina reads to generate a De Bruijn-based assembly graph without any error correction. We then convert the assembly graph to a bluntified sequence graph using VG (Garrison *et al.*, 2017). After graph simplification, the resulting sequence graph has 158,567 nodes and 190,767 edges.

Bubble detection. In the next stage, we use VG's snarl decomposition algorithm (Paten *et al.*, 2017) to detect the regions of heterozygosity, or *snarls*, in the sequence graph. This results in 29,071 bubbles.

PacBio Alignments. After bubble detection, we align different coverage levels ($10\times$, $20\times$ and $30\times$) of long read PacBio data to the generated sequence graph using GraphAligner². This resulted in 21,868, 43,459 and 73,129 PacBio alignments for input coverages of $10\times$, $20\times$ and $30\times$, respectively.

Bubble ordering. To obtain an ordering of bubbles, we perform *de novo* assembly using Canu v1.5 (Koren *et al.*, 2017) on each PacBio dataset. As suggested by Giordano *et al.* (2017), we use Canu v1.5 with the following parameter values: `corMhapSensitivity=high`, `corMinCoverage=2`, `correctedErrorRate=0.10`, `minOverlapLength=499`, `corMaxEvidenceErate=0.3`. Next, we align these Canu contigs to the sequence graph to obtain the bubble ordering, which we define as the sequence of bubbles encountered by each aligned contig. Note that we use Canu solely for bubble ordering. In this paper, we restrict ourselves to phasing bubbles only in unique, non-repetitive regions. We detect repetitive bubbles based on the coverage depth of the PacBio alignments and remove them from downstream analyses. The coverage depth threshold used is 1.67 times the average coverage. This results in 148, 80, and 71 bubble chains, and 26,576, 27,556 and 27,741 bubbles, at coverages of $10\times$, $20\times$, and $30\times$ respectively.

Graph-based phasing. For each of the coverage conditions, we take as input the ordered bubbles, the long-read PacBio alignments and the sequence graph, and solve the gMEC problem by assuming constant weights in the weight matrix \mathcal{W} . The optimal bipartition is computed via backtracing and the final haplotigs are generated by concatenating the node labels of the two optimal paths. These steps have been implemented in our WhatsHap software as a subcommand `phasegraph`³.

3.2 Running Falcon Unzip

The main goal of this study is to measure the performance of phasing using a graph based approach, and, in particular, the quality of haplotypes at heterozygous sites achievable by using this method with low coverage PacBio data. Therefore, we compared our graph-based approach to the state-of-the-art contig based phasing method Falcon Unzip, which also generates diploid assemblies.

The Falcon Unzip (Chin *et al.*, 2016) algorithm first constructs a string graph composed of "haploid consensus" contigs, with bubbles representing structural variant sites between homologous loci. Sequenced reads are then phased and separated for each haplotype on the basis of heterozygous positions. Phased reads are finally used to assemble the backbone sequence (primary contigs) and the alternative haplotype sequences (haplotigs). The combination of primary contigs and haplotigs constitutes the final diploid assembly, which includes phasing information dividing single-nucleotide polymorphisms and structural variants between the two haplotypes.

We ran Falcon Unzip using the parameters given in the official parameter guide⁴. We tried to run Falcon Unzip for lower coverages of $10\times$ and $20\times$, but it did not generate output in these cases (and we assume it is not designed for such low coverages). Therefore, we only ran Falcon Unzip for $20\times$ PacBio coverage. Primary contigs and haplotigs were polished using the Quiver algorithm and corrected for SNPs and indels using Illumina data via Pilon, with the parameters `--diploid` and `--fix all` (Walker *et al.*, 2014).

² <https://github.com/maickrau/GraphAligner>

³ Presently this functionality resides in the MAV branch, which will be merged to the master branch in the near future and will be part of future WhatsHap releases.

⁴ <http://pb-falcon.readthedocs.io/en/latest/parameters.html>

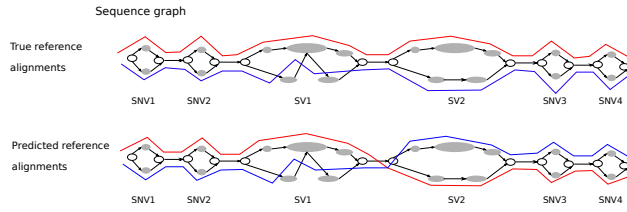


Fig. 5. For a subgraph of G_s , this example shows the true (top) and predicted (bottom) versions of two haplotype alignments (red and blue) through a series of bubbles. When comparing the correspondingly-colored lines between the two versions, we see one switch between SV1 and SV2: the prediction contains one switch error. Six bubbles have been phased, for a total of five phase connections between consecutive bubbles. Therefore, the phasing error rate is $1/5$.

Statistics	PacBio coverage	Graph-based approach	Falcon Unzip
Diploid assemblies Quality			
Average Identity[%]	10×	99.50	—
	20×	99.61	—
	30×	99.80	99.4
Phasing error rate[%]	10×	2.5	—
	20×	1.5	—
	30×	0.7	3.8
Contiguity			
N50 haplotig size [bp]	10×	40k	—
	20×	42k	—
	30×	43k	32k
Completeness			
Haplotig size [Mbp]	10×	20.7	—
	20×	21.1	—
	30×	23.9	16.6
# Unphased contigs	10×	2	—
	20×	2	—
	30×	2	77

Table 1. Comparison of two phasing methods, Falcon Unzip and our graph-based approach, at different PacBio coverage levels. For computing the “haplotig N50”, we only consider those portions of a contig for which two haplotypes are available, i.e. those regions where Falcon reports both a primary contig and an alternative haplotig. For “haplotig size”, we sum the length of contigs on both haplotypes (“primary contigs” plus “haplotigs” in terms of Falcon’s output), so the target size is twice the genome size (24.3Mbp in case of yeast).

3.3 Assembly performance assessment

To evaluate the accuracy of the predicted haplotypes, we align reference assemblies of the two yeast strains SK1 and Y12 (Yue *et al.*, 2017) to the sequence graph. We emphasize that these reference assemblies are only used for evaluation purposes and are not a part of our assembly pipeline. We use the following performance measures for the evaluation of diploid assemblies:

Phasing error rate. Over the yeast genome, we compare the different diploid assemblies with the ground truth haploid genomes of SK1 and Y12. As with the reference assemblies, we align the haplotigs produced by Falcon Unzip to our sequence graph. For each phased bubble chain, the predicted haplotype is expressed as a mosaic of the two true haplotypes, minimizing the number of switches. This minimum then gives the number of switch errors. The phasing error rate is defined as the number of switch errors divided by the number of phased bubbles. Figure 5 illustrates this calculation for a toy example. The top panel shows the true references aligned to the sequence graph. At the bottom, predicted haplotypes (from

Falcon Unzip or our graph-based approach) are aligned to the graph. Comparing the true and predicted haplotypes, we see one switch between SV1 and SV2, which means that the switch error count is one. The number of phase connections between consecutive bubbles is five and the resulting switch error rate for this example is $1/5$.

Average Percent Identity. We consider the best assignment of each haplotig to either of the two true references, obtained by aligning the haplotig to the references. For each whole diploid assembly, we compute the average of the best-alignment percent identities over all haplotigs.

Assembly contiguity. We assess the contiguity of the assemblies by computing the N50 of haplotig size.

Assembly completeness. We consider two assembly completeness statistics: first, the total length of haplotigs assembled by each method, and second, the total number of unphased contigs.

4 Results

In this section, we present the results of our analysis of the diploid assemblies generated by our method and by Falcon Unzip on the data sets described above.

Coverage analysis. To discover a cost-effective method for assembling a diploid genome, we consider PacBio datasets that vary in terms of coverage—specifically, 10×, 20× and 30× coverage are considered. One of the primary aims of our study is to compare two approaches—the graph-based approach we implemented and the contig-based phasing done by Falcon Unzip. In doing so, we quantify the agreement between the diploid assemblies generated by both methods and the true references. Table 1 shows the assembly performance statistics for both of these methods. In order to assess the accuracy of the competing diploid assemblies, we compute the phasing error rate and the average percent identity at different PacBio coverages. For the graph-based approach, we observe that as we increase the long read coverage from 10× to 30×, the average identity of haplotigs increases from 99.5% to 99.8% and the phasing error rate decreases from 2.5% to 0.7%. In contrast, Falcon Unzip produces haplotigs with an average identity of 99.4% and phasing error rate of 3.8% at 30× coverage. Overall, comparing the agreement between the graph-based approach (at 10× coverage) and Falcon Unzip (at 30× coverage) to the true references, our graph-based approach delivers better haplotigs with respect to all measures reported in Table 1. We believe that one reason for this is that we use an Illumina-based graph as a backbone. Furthermore, solving the gMEC formulation for phasing optimally most likely contributes to generating accurate haplotigs. Overall, our analysis supports the conclusion that our approach delivers accurate haplotype sequences even at a long read coverage as low as 10×.

To analyse the effect of different coverages of the Illumina short-read datasets on the quality of our haplotigs, we went back to the original (high coverage) Illumina dataset and downsampled it to 100× coverage, i.e. twice the amount of reads used above. We observe that increasing the coverage does not have drastic effect on the quality of haplotigs. The average phasing identity rose to 99.81% and the total haplotig size is 23.9Mbp, which is virtually identical to the results for 50× reported in Table 1.

With an increase in average PacBio coverage from 10× to 30×, the haplotype contiguity achievable by using our approach improves from 40kbp to 43kbp. By way of comparison, Falcon Unzip delivers haplotigs with a N50 length of 32kbp at the same coverage level. This highlights the fact that our approach generates more contiguous haplotypes compared to Falcon Unzip. In terms of haplotype completeness, our approach yields diploid assemblies of length 20.7 Mbp, 21.1 Mbp and 23.9 Mbp at average PacBio coverages of 10×, 20× and 30× respectively. At coverage 30×, Falcon Unzip delivers a total assembly size of 16.6Mbp, while the total length of both haplotypes of the pseudo-diploid yeast genome is 24.3 Mbp.

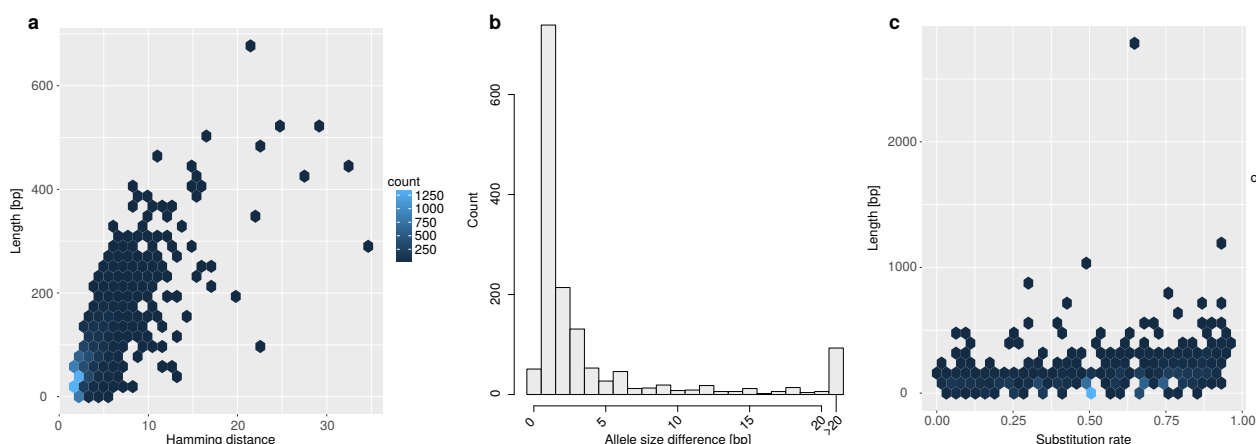


Fig. 6. Structural variation analysis of phased bubbles from our graph-based approach. a: Joint distribution of allele length and Hamming distance, for pure substitutions. b: Distribution of size difference between the two alleles, for mixed bubbles and indels. Pure substitutions always have a size difference of 0, and are not included in the figure. c: Joint distribution of the length of the longer allele and the substitution rate, for mixed bubbles. With a higher substitution rate, the bubble has more substitutions, and with a lower rate more indels.

Our approach therefore delivers more complete haplotypes at a long-read coverage of $10\times$ compared to Falcon Unzip at a coverage of $30\times$. There are 2 haplotigs that are not phased by our approach; this is due to the lack of heterozygosity over those regions. On the other hand, there are 77 (out of 123) contigs that are not phased by Falcon Unzip. In summary, the graph-based approach delivers complete and contiguous haplotype sequences even at a low coverage of $10\times$.

Bubble characterization. Our next aim is to characterize the nature of the heterozygous genomic variation encoded in the phased bubbles. There are 25,033 bi-allelic bubbles phased by our approach when using $30\times$ coverage PacBio data. Of these bubbles, there are 15,293 for which both allele sequences have a length of at most 1 bp, out of which 15,258 are single base pair substitutions (SNVs) and 35 are 1 bp indels. The remaining 9,740 bubbles either encode two or more small variants or more complex differences. To differentiate these cases, we computed an alignment between the two allele paths and refer to those bubbles for which the alignment contains only substitutions but no indels as “pure substitutions”. Figure 6a shows the joint distribution of length and (Hamming) distance for these pure substitution bubbles. This analysis reveals, on the one hand, that many longer pure substitutions have a low distance and hence encode multiple SNVs and, on the other hand, that there also exists a population of more complex substitutions. For the 1,489 bubbles not classified as pure substitutions, which we refer to as “mixed bubbles”, Figure 6b shows the absolute length difference between the two alleles. While this difference is small for most bubbles, there are 93 bubbles with a length difference of 21 bp or more. To further elucidate the nature of the sequence differences, Figure 6c presents the joint distribution of length of the longer allele and substitution rate, which is defined as the fraction of substitutions among all edit operations done to align the two sequences. That is, a pure insertion or deletion has a substitution rate of 0.

5 Discussion

The Falcon Unzip method (Chin *et al.*, 2016) is purely based on PacBio data, which exhibit a high error rate, and is therefore not suitable for lower coverages. By using (costly) high coverage PacBio data, Falcon Unzip can generate good quality assemblies with an average haplotig identity of up to 99.99% (Chin *et al.*, 2016). However, it follows a conservative approach for phasing genomic variants: As sketched in Figure 2, Falcon Unzip generates long primary contigs, but tends to phase them only partially.

To address the above problems, we have provided a novel graph-based approach to diploid genome assembly by combining different

sequencing technologies. By using one technology producing shorter, more accurate reads, and a second technology delivering long reads, we jointly produce accurate, complete and contiguous haplotypes. In doing so, we also provided a cost-effective way of generating high quality diploid assemblies. By performing phasing directly in the space of sequence graphs—without flattening them to contigs in intermediate steps—we can phase large structural variants, which was not possible in linear approaches. We have tested our approach using real data for a pseudo-diploid yeast genome, and shown that we deliver accurate and complete haplotigs. We have shown that we can detect and phase structural variants.

In this study, our main focus was to phase unique regions of the genome. As a next step, we plan to look into repetitive regions and phase them as well. To this end, it is important to note that resolving repeats and polyploid phasing are closely related problems, as pointed out by Chaisson *et al.* (2017a). Therefore, we will aim to solve heterozygous variants and repeats in a joint phasing framework, in order to obtain even more contiguous diploid genome assemblies that include both types of features. That would also remove the need of running an external assembler (Canu) for bubble ordering. Finally, our framework allows, in principle, for incorporating more data from other sequencing technologies, like chromatin-conformation capture (Burton *et al.*, 2013), linked read sequencing (Weisenfeld *et al.*, 2017), and single-cell template strand sequencing (Strand-seq; Porubský *et al.*, 2016). In previous studies on reference-based haplotyping, we have shown such integrative approaches to be very powerful in obtaining chromosome-scale haplotypes (Porubský *et al.*, 2017; Chaisson *et al.*, 2017b), which we believe can be lifted to *de novo* diploid genome assemblies.

Acknowledgements We thank Ali Ghaffaari for providing the pystream module and Benedict Paten for inspiring discussions.

References

- Antipov, D., Korobeynikov, A., McLean, J. S., and Pevzner, P. A. (2015). hybridspades: an algorithm for hybrid assembly of short and long reads. *Bioinformatics*, **32**(7), 1009–1015.
- Bankevich, A., Nurk, S., Antipov, D., Gurevich, A. A., Dvorkin, M., Kulikov, A. S., Lesin, V. M., Nikolenko, S. I., Pham, S., Prjibelski, A. D., *et al.* (2012). Spades: a new genome assembly algorithm and its applications to single-cell sequencing. *Journal of computational biology*, **19**(5), 455–477.
- Bashir, A., Klammer, A. A., Robins, W. P., Chin, C.-S., Webster, D., Paxinos, E., Hsu, D., Ashby, M., Wang, S., Peluso, P., *et al.* (2012). A hybrid approach for the automated finishing of bacterial genomes. *Nature biotechnology*, **30**(7), 701–707.
- Berlin, K., Koren, S., Chin, C.-S., Drake, J. P., Landolin, J. M., and Phillippy, A. M. (2015). Assembling large genomes with single-molecule sequencing and locality-sensitive hashing. *Nature biotechnology*, **33**(6), 623–630.

- Burton, J. N., Adey, A., Patwardhan, R. P., Qiu, R., Kitzman, J. O., and Shendure, J. (2013). Chromosome-scale scaffolding of de novo genome assemblies based on chromatin interactions. *Nature biotechnology*, **31**(12), 1119–1125.
- Chaisson, M. J., Mukherjee, S., Kannan, S., and Eichler, E. E. (2017a). Resolving multicopy duplications de novo using polyploid phasing. In *International Conference on Research in Computational Molecular Biology*, pages 117–133. Springer.
- Chaisson, M. J. P., Sanders, A. D., Zhao, X., Malhotra, A., Porubsky, D., Rausch, T., and et al. (2017b). Multi-platform discovery of haplotype-resolved structural variation in human genomes.
- Chin, C.-S., Alexander, D. H., Marks, P., Klammer, A. A., Drake, J., Heiner, C., Clum, A., Copeland, A., Huddleston, J., Eichler, E. E., et al. (2013). Nonhybrid, finished microbial genome assemblies from long-read smrt sequencing data. *Nature methods*, **10**(6), 563–569.
- Chin, C.-S., Peluso, P., Sedlazeck, F. J., Nattestad, M., Concepcion, G. T., Clum, A., Dunn, C., OâL™Malley, R., Figueroa-Balderas, R., Morales-Cruz, A., et al. (2016). Phased diploid genome assembly with single molecule real-time sequencing. *Nature methods*, **13**(12), 1050.
- Cilibrasi, R., Van Iersel, L., Kelk, S., and Tromp, J. (2007). The complexity of the single individual snp haplotyping problem. *Algorithmica*, **49**(1), 13–36.
- Garrison, E., Sirén, J., Novak, A. M., Hickey, G., Eizenga, J. M., Dawson, E. T., Jones, W., Lin, M. F., Paten, B., and Durbin, R. (2017). Sequence variation aware genome references and read mapping with the variation graph toolkit. *bioRxiv*, page 234856.
- Giordano, F., Aigrain, L., Quail, M. A., Coupland, P., Bonfield, J. K., Davies, R. M., Tischler, G., Jackson, D. K., Keane, T. M., Li, J., et al. (2017). De novo yeast genome assemblies from minion, pacbio and miseq platforms. *Scientific reports*, **7**.
- Glusman, G., Cox, H. C., and Roach, J. C. (2014). Whole-genome haplotyping approaches and genomic medicine. *Genome medicine*, **6**(9), 73.
- Hunt, M., De Silva, N., Otto, T. D., Parkhill, J., Keane, J. A., and Harris, S. R. (2015). Circlator: automated circularization of genome assemblies using long sequencing reads. *Genome biology*, **16**(1), 294.
- Idury, R. M. and Waterman, M. S. (1995). A new algorithm for dna sequence assembly. *Journal of computational biology*, **2**(2), 291–306.
- Kajitani, R., Toshimoto, K., Noguchi, H., Toyoda, A., Ogura, Y., Okuno, M., Yabana, M., Harada, M., Nagayasu, E., Maruyama, H., et al. (2014). Efficient de novo assembly of highly heterozygous genomes from whole-genome shotgun short reads. *Genome research*, **24**(8), 1384–1395.
- Klau, G. W. and Marschall, T. (2017). A guided tour to computational haplotyping. In *Conference on Computability in Europe*, pages 50–63. Springer.
- Koren, S., Walenz, B. P., Berlin, K., Miller, J. R., Bergman, N. H., and Phillippy, A. M. (2017). Canu: scalable and accurate long-read assembly via adaptive k-mer weighting and repeat separation. *Genome research*, **27**(5), 722–736.
- Lancia, G., Bafna, V., Istrail, S., Lippert, R., and Schwartz, R. (2001). SNPs problems, complexity, and algorithms. In F. M. a. d. Heide, editor, *Algorithms ÅcÅLÅ” ESA 2001*, number 2161 in Lecture Notes in Computer Science, pages 182–193. Springer Berlin Heidelberg.
- Levy, S., Sutton, G., Ng, P. C., Feuk, L., Halpern, A. L., Walenz, B. P., Axelrod, N., Huang, J., Kirkness, E. F., Denisov, G., et al. (2007). The diploid genome sequence of an individual human. *PLoS biology*, **5**(10), e254.
- Li, H. (2015a). Bfc: correcting illumina sequencing errors. *Bioinformatics*, **31**(17), 2885–2887.
- Li, H. (2015b). Fermikit: assembly-based variant calling for illumina resequencing data. *Bioinformatics*, **31**(22), 3694–3696.
- Lin, Y., Yuan, J., Kolmogorov, M., Shen, M. W., Chaisson, M., and Pevzner, P. A. (2016). Assembly of long error-prone reads using de bruijn graphs. *Proceedings of the National Academy of Sciences*, **113**(52), E8396–E8405.
- Lippert, R., Schwartz, R., Lancia, G., and Istrail, S. (2002). Algorithmic strategies for the single nucleotide polymorphism haplotype assembly problem. *Briefings in Bioinformatics*, **3**(1), 23–31.
- Martin, M., Patterson, M., Garg, S., Fischer, S. O., Pisanti, N., Klau, G. W., Schoenhuth, A., and Marschall, T. (2016). Whatshap: fast and accurate read-based phasing. *bioRxiv*, page 085050.
- Medvedev, P., Georgiou, K., Myers, G., and Brudno, M. (2007). Computability of models for sequence assembly. In *WABI*, volume 4645, pages 289–301. Springer.
- Mostovoy, Y., Levy-Sakin, M., Lam, J., Lam, E. T., Hastie, A. R., Marks, P., Lee, J., Chu, C., Lin, C., Džakula, Ž., et al. (2016). A hybrid approach for de novo human genome sequence assembly and phasing. *Nature methods*, **13**(7), 587.
- Myers, E. W. (1995). Toward simplifying and accurately formulating fragment assembly. *Journal of Computational Biology*, **2**(2), 275–290.
- Myers, E. W. (2005). The fragment assembly string graph. *Bioinformatics*, **21**(suppl_2), ii79–ii85.
- Nagarajan, N. and Pop, M. (2009). Parametric complexity of sequence assembly: theory and applications to next generation sequencing. *Journal of computational biology*, **16**(7), 897–908.
- Nagarajan, N. and Pop, M. (2013). Sequence assembly demystified. *Nature Reviews Genetics*, **14**(3), 157–167.
- Paten, B., Novak, A. M., Garrison, E., and Hickey, G. (2017). Superbubbles, ultrabubbles and cacti. In *International Conference on Research in Computational Molecular Biology*, pages 173–189. Springer.
- Patterson, M., Marschall, T., Pisanti, N., van Iersel, L., Stougie, L., Klau, G. W., and Schönhuth, A. (2014). Whatshap: Haplotype assembly for future-generation sequencing reads. In *RECOMB*, volume 8394, pages 237–249. Springer.
- Pendleton, M., Sebra, R., Pang, A. W. C., Ummat, A., Franzen, O., Rausch, T., Stütz, A. M., Stedman, W., Anantharaman, T., Hastie, A., et al. (2015). Assembly and diploid architecture of an individual human genome via single-molecule technologies. *Nature methods*, **12**(8), 780–786.
- Pevzner, P. A., Tang, H., and Waterman, M. S. (2001). An eulerian path approach to dna fragment assembly. *Proceedings of the National Academy of Sciences*, **98**(17), 9748–9753.
- Porubský, D., Sanders, A. D., Vietmarschen, N. v., Falconer, E., Hills, M., Spierings, D. C. J., Bevova, M. R., Guryev, V., and Lansdorp, P. M. (2016). Direct chromosome-length haplotyping by single-cell sequencing. *Genome Res.*
- Porubsky, D., Garg, S., Sanders, A. D., Korb, J. O., Guryev, V., Lansdorp, P. M., and Marschall, T. (2017). Dense and accurate whole-chromosome haplotyping of individual genomes. *Nature Communications*, **8**(1), 1293.
- Pryszcz, L. P. and Gabaldón, T. (2016). Redundans: an assembly pipeline for highly heterozygous genomes. *Nucleic acids research*, **44**(12), e113–e113.
- Rautiainen, M. and Marschall, T. (2017). Aligning sequences to general graphs in o (v+ me) time. *bioRxiv*, page 216127.
- Rhee, J.-K., Li, H., Joung, J.-G., Hwang, K.-B., Zhang, B.-T., and Shin, S.-Y. (2016). Survey of computational haplotype determination methods for single individual. *Genes & Genomics*, **38**(1), 1–12.
- Seo, J.-S., Rhie, A., Kim, J., Lee, S., Sohn, M.-H., Kim, C.-U., Hastie, A., Cao, H., Yun, J.-Y., Kim, J., et al. (2016). De novo assembly and phasing of a korean human genome. *Nature*, **538**(7624), 243–247.
- Simpson, J. T. and Durbin, R. (2012). Efficient de novo assembly of large genomes using compressed data structures. *Genome research*, **22**(3), 549–556.
- Sović, I., Skala, K., and Šikić, M. (2013). Approaches to dna de novo assembly. In *Information & Communication Technology Electronics & Microelectronics (MIPRO), 2013 36th International Convention on*, pages 351–359. IEEE.
- Tewhey, R., Bansal, V., Torkamani, A., Topol, E. J., and Schork, N. J. (2011). The importance of phase information for human genomics. *Nature reviews. Genetics*, **12**(3), 215.
- Vaser, R., Sović, I., Nagarajan, N., and Šikić, M. (2017). Fast and accurate de novo genome assembly from long uncorrected reads. *Genome research*, **27**(5), 737–746.
- Vinson, J. P., Jaffe, D. B., O’Neill, K., Karlsson, E. K., Stange-Thomann, N., Anderson, S., Mesirov, J. P., Satoh, N., Satou, Y., Nusbaum, C., et al. (2005). Assembly of polymorphic genomes: algorithms and application to ciona savignyi. *Genome research*, **15**(8), 1127–1135.
- Walker, B. J., Abeel, T., Shea, T., Priest, M., Abouelliel, A., Sakthikumar, S., Cuomo, C. A., Zeng, Q., Wortman, J., Young, S. K., et al. (2014). Pilon: an integrated tool for comprehensive microbial variant detection and genome assembly improvement. *PLoS one*, **9**(11), e112963.
- Weisenfeld, N. I., Kumar, V., Shah, P., Church, D. M., and Jaffe, D. B. (2017). Direct determination of diploid genome sequences. *Genome research*, **27**(5), 757–767.
- Xiao, C.-L., Chen, Y., Xie, S.-Q., Chen, K.-N., Wang, Y., Luo, F., and Xie, Z. (2016). Mecat: an ultra-fast mapping, error correction and de novo assembly tool for single-molecule sequencing reads. *bioRxiv*, page 089250.
- Yue, J.-X., Li, J., Aigrain, L., Hallin, J., Persson, K., Oliver, K., Bergström, A., Coupland, P., Warringer, J., Lagomarsino, M. C., et al. (2017). Contrasting evolutionary genome dynamics between domesticated and wild yeasts. *Nature genetics*, **49**(6), 913–924.
- Zimin, A. V., Puiu, D., Luo, M.-C., Zhu, T., Koren, S., Marçais, G., Yorke, J. A., Dvořák, J., and Salzberg, S. L. (2017). Hybrid assembly of the large and highly repetitive genome of aegilops tauschii, a progenitor of bread wheat, with the masurca mega-reads algorithm. *Genome Research*, **27**(5), 787–792.